Nuclear Inst. and Methods in Physics Research, A 1047 (2023) 167829

Contents lists available at ScienceDirect

Nuclear Inst. and Methods in Physics Research, A

journal homepage: www.elsevier.com/locate/nima

Modeling and implementation of vertical excursion FFA in the Zgoubi ray-tracing code

Marion Vanwelde [a,*], Cédric Hernalsteens [a,b,**], François Méot [c], Nicolas Pauly [a], Robin Tesse [a]

[a] Service de Métrologie Nucléaire (CP165/84), Université libre de Bruxelles, Avenue Franklin Roosevelt 50, 1050 Brussels, Belgium
[b] CERN, European Organization for Nuclear Research, Esplanade des Particules 1, 1211 Meyrin, Switzerland
[c] Collider Accelerator Department, Brookhaven National Laboratory, Long Island, Upton, NY, USA

ARTICLE INFO

Keywords:
Fixed Field Accelerator
Vertical orbit excursion FFA
Ray-tracing code

ABSTRACT

Vertical Fixed Field Accelerators (vFFAs) feature complex and highly non-linear magnetic fields, which require simulation codes allowing step-wise particle tracking. Methods to model the 3D magnetic field of scaling vFFAs have been developed in the ray-tracing code Zgoubi. The field modeling and particle tracking methods include the field non-linearities, the fringe fields, and the field superposition of neighboring magnets. The procedure implements the vFFA analytical field expressions, allowing design studies and parameter optimizations using the Zgoubi built-in fit method. The vFFA procedure has been applied to a ten-fold symmetry ring with a triplet focusing structure designed to accelerate protons from 3 MeV to 12 MeV and studied under the ISIS-II proton driver prototype project. Results from particle tracking in externally generated 3D semi-analytical field maps and the developed vFFA analytical model are shown to be in excellent agreement.

1. Introduction

Vertical Fixed Field Accelerators (vFFAs) [1,2] feature magnetic fields increasing exponentially in the vertical direction, such that the higher energy particle orbits are stacked vertically. Recently, these vFFAs have regained interest and have been considered for various applications, from nuclear waste transmutation to energy-recovery electron accelerators [1]. As part of the ISIS upgrade project ("ISIS-II") at the ISIS Neutron and Muon Source Facility [3–5], vFFAs have been identified as potential candidates for the 1.2 GeV proton driver of the neutron and muon source [6]. The design procedure of such a vFFA prototype ring has been studied in detail in Ref. [2]. In this context, tools are necessary to model vFFA scaling magnets with high accuracy, optimize their parameters, and track particles in their complex and highly non-linear magnetic fields.

The ray-tracing code Zgoubi [7–9] allows step-by-step particle tracking in arbitrary electric and magnetic fields. It provides realistic field models accounting for the lattice element fringe fields and possible misalignments. Its fitting procedure facilitates magnet parameter optimization based on the accelerator requirements. All these features place Zgoubi as a leading simulation code to study vFFAs. The linear optics of the vFFA lattice considered for the ISIS-II upgrade [2] has been performed and compared using codes dedicated to fixed-field accelerators (SCODE+ [10] and FixField [11]). On the other hand, Zgoubi has been used in important FFA studies, such as RACCAM [12], EMMA [13], and PAMELA [14], demonstrating its ability to study the beam dynamics of these complex configurations. Equipping Zgoubi with a dedicated vFFA routine is essential to benefit from the vast capabilities of Zgoubi to cross-validate vFFA design studies with other codes. The flexibility of Zgoubi allows simulating numerous physics processes, such as beam-gas interactions, spin tracking, and synchrotron radiation. Our implementation of the vFFA keyword makes vFFAs first-class elements in Zgoubi. Additionally, this makes it possible to use a single code at different stages of the study by first using the newly implemented model, and seamlessly switching to computed or measured field maps within the same simulation packages at later stages. The analytical models of SCODE+ and FixField are used to benchmark and validate our results.

We detail the development of a Zgoubi procedure to track particles in vFFA cells. This procedure is then used and benchmarked to study a ten-cell lattice composed of three vFFA magnets per cell (triplet focusing structure). This lattice corresponds to the first design of the vFFA proton driver prototype (FETS-FFA) studied under the ISIS-II project [2,6]. The vFFA field model implemented in Zgoubi allows for studying the linear and non-linear beam dynamics, including the closed orbit search, the tune computation, and the dynamic aperture study. The vFFA analytical model can also facilitate the design of arbitrary vFFA lattices, from studying stability limits to field and alignment error studies. In addition, Zgoubi allows tracking particles in externally provided

* Corresponding author.
** Corresponding author at: Service de Métrologie Nucléaire (CP165/84), Université libre de Bruxelles, Avenue Franklin Roosevelt 50, 1050 Brussels, Belgium.
E-mail addresses: marion.vanwelde@ulb.be (M. Vanwelde), cedric.hernalsteens@cern.ch (C. Hernalsteens).

https://doi.org/10.1016/j.nima.2022.167829
Received 23 August 2022; Received in revised form 4 November 2022; Accepted 18 November 2022
Available online 21 November 2022

3D field maps. A comparison between particle tracking in 3D semi-analytical field maps—field maps built from the analytical expressions but requiring the additional interpolation step from a fixed mesh—and the implemented vFFA analytical model is performed and discussed in detail to validate the implementation of the new vFFA Zgoubi keyword.

The structure of the paper is as follows. Section 2 describes the procedure implemented to model vFFAs, detailing the model parameters and the procedure specificities. Section 3 illustrates the procedure on the 3 MeV vFFA ring based on a FDF cell and validates the effectiveness of the method by comparing with results obtained from particle tracking in an externally generated 3D field map. Finally, conclusions on the performance and benefits of the implemented vFFA keyword are provided in Section 4.

2. The vFFA procedure

To compute the particle motion in arbitrary magnetic fields, Zgoubi solves the Lorentz equation at each numerical integration step using truncated Taylor series (truncation at the fifth and sixth order to compute the particle position and velocity) [15,16]. By contrast, other general-purpose simulation codes such as OPAL [17] and Geant4 [18] perform integration in field maps using standard numerical integration techniques. Although non-symplectic in nature, this key peculiarity of the integration algorithm in Zgoubi provides a reduced loss of symplecticity in tracking results and represents a distinguishing feature. The Taylor series coefficients can be computed when the magnetic field $B(X, Y, Z)$ and its derivatives $\partial^{k+l+m}\mathbf{B}/\partial X^k \partial Y^l \partial Z^m$ are known at each point in the 3D space [7,16]. The magnetic field is obtained either from built-in analytical models in the source code or from user-provided field maps. The analytical models provide the magnetic field components for arbitrary coordinates (X, Y, Z). In contrast, the user-provided field map contains the magnetic field components on a pre-defined mesh. Zgoubi then performs a polynomial interpolation to compute the magnetic field and derivatives at the particle position. For the numerical integration, Zgoubi treats the beamline elements separately and successively. Two methods exist to account for the possible influence of neighboring magnets. The first method involves placing several similar magnets in the Zgoubi element to exactly superpose their magnetic field contribution (N-uplet elements such as the "FFAG" and "FFAG-SPI" Zgoubi keywords which represent conventional horizontal excursion, radial or spiral type, FFA elements [15,19]). The second method sets an integration zone greater than the element extent to linearly superpose the neighboring cell residual fields (as for the cartesian elements [16]). This section details the implementation of the vFFA analytical model in the Zgoubi source code. Both methods to account for the possible overlapping field contribution of neighboring magnets have been implemented in the vFFA procedure. In this respect, vFFA elements can contain multiple vFFA magnets (possibly defining a complete cell), and their integration limits can be extended to account for the influence of neighboring cells.

The definition of the new vFFA procedure is shown in Fig. 1 as it should appear in the Zgoubi input file. The implemented vFFA Zgoubi keyword can contain up to five vFFA magnets in its integration zone, allowing the superposition of the magnetic fields from neighboring magnets in the same cell. The vFFA procedure represents a multi-magnet in a Cartesian reference frame, in which the placement and length of each magnet are provided by the parameters XM_i (magnet start position) and L_i (magnet length), as shown in Fig. 2. The parameter XL defines the total extent of the element. This element contains the N vFFA magnets and considers the fringe fields of all these magnets. The vFFA magnets inside the element can be offset from each other by setting the DYM_i and DZM_i parameters. To account for the overlapping residual fields coming from neighboring cells, the user can define an integration zone greater than the cell extent by setting the XE and XS parameters in the vFFA definition. Zgoubi will therefore integrate from -XE to XL+XS. Setting such integration limits assumes that the field is small enough to ensure that the particle trajectory deviation due to the residual field is limited so that the first-order field superposition with possible upstream and/or downstream similar residual fields (adjacent vFFA cells for instance) is valid. These integration limits become very useful when the fringe fields are dominating the field profiles along the cell, and the neighboring cell residual field is large enough to influence the optical properties of the lattice, as will be the case for the lattice studied in Section 3.

```
'vFFA'
IL,
N (Number of vFFA magnets), XL (Total length of the component),
XE, XS (Entrance/exit integration zones)
-----------For each vFFA magnet:------------------------------
  XM (Magnet start position), L (Magnet length), DYM,
    DZM (Magnet transverse offsets)
  B0 (Reference magnetic field), k (Normalised field gradient),
  gap (Fringe field extent)
--------------------------------------------------------------
KIRD, Resol, (Only KIRD = 0 - analytical computation)
XPAS (Integration step),
KPOS, XCE, YCE, ALE (Positioning of the element)
```

Fig. 1. The vFFA definition with its associated parameters, ordered as it should appear in the Zgoubi input file.

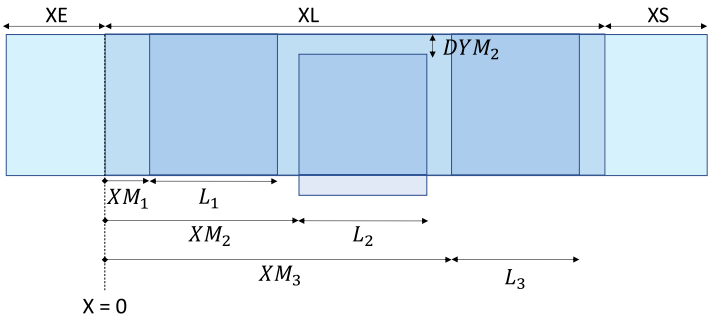

Fig. 2. The vFFA procedure implemented in Zgoubi. The vFFA element is defined in Cartesian coordinates and can contain multiple vFFA magnets. These magnets are placed via the XM_i parameters, and the L_i parameters give their respective lengths. The magnets can be horizontally and vertically offset from each other using respectively the DYM_i and DZM_i parameters, allowing misalignment studies. The tracking of the particles in such an element is done from -XE to XL+XS, considering the overlapping residual field of neighboring cells.

The magnetic field of a vFFA magnet satisfies the scaling condition $B = B_0 \exp[k(z - z_0)]$ for all its components, where $k = (1/B)(\partial B/\partial z)$ is the normalized field gradient, z_0 is a reference vertical position and B_0 is the bending field at that reference position. The magnetic field increases exponentially in the vertical direction so that higher energy particle orbits will move vertically. This behavior differs from the conventional horizontal excursion FFAs, in which the orbits of the particles at higher momentum move horizontally. In what follows, x is the longitudinal coordinate, y is the horizontal coordinate, and z is the vertical coordinate. Considering the fringe field function $g(x)$, the three field components in the vertical median plane are:

$$B_{y0}(x, 0, z) = 0, \tag{1}$$

$$B_{z0}(x, 0, z) = B_0 e^{kz} g(x), \tag{2}$$

$$B_{x0}(x, 0, z) = \frac{B_0}{k} e^{kz} \frac{dg}{dx}. \tag{3}$$

The function $g(x)$ gives the longitudinal dependence of the field and represents the fringe field of the magnets. In the procedure implemented in the source code, no pole face angles are considered for vFFA magnets.

Two methods exist in the Zgoubi Fortran source code to implement the analytical magnetic field model of an element at any point in the 3D space. The first method consists in defining the magnetic field in the magnet median plane and using the Zgoubi extrapolation routine (which assumes a conventional horizontal midplane) to obtain out-of-plane field components respecting Maxwell's equations. The second method directly provides the expressions of the magnetic field and its derivatives at any point (X, Y, Z) in the 3D space. We used the second method to implement the vFFA keyword because the median plane in a vFFA magnet is vertical, implying necessary changes in the extrapolation procedure if the first method was used. Assuming $z_0 = 0$, the magnetic field of a vFFA magnet at any position (X, Y, Z) in the 3D space can be described with an out-of-plane expansion [2]:

$$B_x(x,y,z) = B_0 e^{kz} \sum_{i=0}^{n} b_{xi}(x) y^i, \tag{4}$$

$$B_y(x,y,z) = B_0 e^{kz} \sum_{i=0}^{n} b_{yi}(x) y^i, \tag{5}$$

$$B_z(x,y,z) = B_0 e^{kz} \sum_{i=0}^{n} b_{zi}(x) y^i, \tag{6}$$

where the coefficients of these equations are given by recurrence relations [2]:

$$b_{y0}(x) = 0, \qquad b_{y,i+1}(x) = -\frac{1}{i+1}\left(k b_{zi} + \frac{d b_{xi}}{dx}\right),$$

$$b_{z0}(x) = g(x), \qquad b_{z,i+2}(x) = \frac{k}{i+2} b_{y,i+1},$$

$$b_{x0}(x) = \frac{1}{k}\frac{dg}{dx}, \qquad b_{x,i+2}(x) = \frac{1}{i+2}\frac{d b_{y,i+1}}{dx}.$$

To develop the magnetic field outside the median plane, we truncated this series at the 8th or 10th order and compared their difference, as we will see in Section 3. Furthermore, we also compared these results with higher-order truncations obtained in field maps and showed convergence for an out-of-plane expansion truncation at the 10th order. We will see that the truncation order influences the Maxwellian character of the magnetic field, especially when deviating significantly from the median plane. If the series given in Eqs. (4)–(6) is infinite, the out-of-plane expansion would satisfy Maxwell's equations exactly, while the truncation slightly alters the field Maxwellian property.

2.1. Field fall-offs

The function $g(x)$ represents the fringe field of vFFA magnets. In the procedure implemented in Zgoubi, the fringe field is modeled by a hyperbolic tangent function:

$$g(x) = \frac{1}{2}\left[\tanh\left(\frac{x}{h_g}\right) - \tanh\left(\frac{x - L_{\text{mag}}}{h_g}\right)\right], \tag{7}$$

where h_g represents the fringe field extent and is independent of the coordinates. The fringe fields at the magnet entrance and exit are identical. The hyperbolic tangent function is often used to describe the fringe field in vFFAs [1,2]. For this reason, we decided to use this form of fringe field. However, given the few studies on vFFA magnets, it is not certain that this fringe field correctly describes a realistic field shape [20]. Further development must be conducted to verify that it can match the field fall-off of proper 3D magnet computation code. An external code using the Python library Sympy [21] has been developed, allowing quickly changing the fringe field function to match the 3D field distribution when more in-depth studies on realistic magnets are carried out. Using this external code, the analytical expressions of the magnetic field and derivatives can be readily regenerated for arbitrary changes in the fringe field function and then set in the Fortran source code.

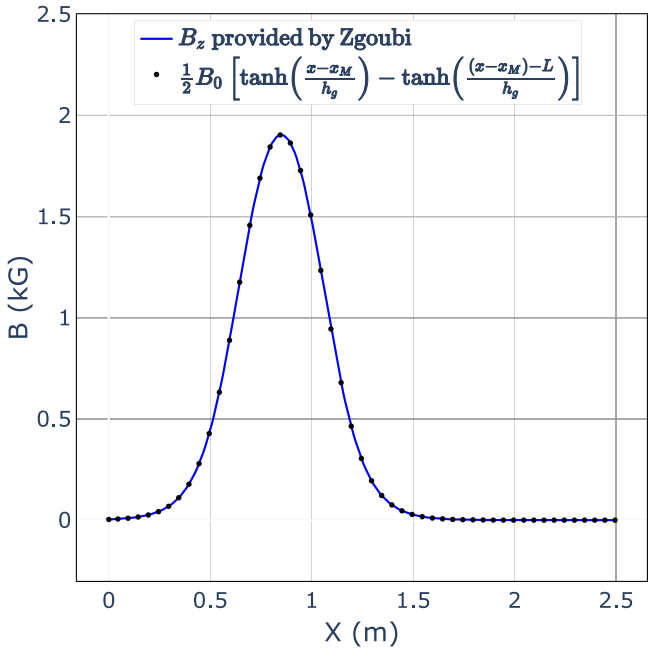

Fig. 3. Vertical magnetic field along a straight line crossing a vFFA magnet which corresponds to the first magnet of the FDF triplet described in Ref. [2]. The markers correspond to the analytically calculated fringe field function, while the solid curve corresponds to the field returned by Zgoubi, which is the field as observed by a particle along a straight line. The horizontal and vertical coordinates remain zero; the field corresponds to the midplane field and has the form $B_0 \times g(x)$. It is thus proportional to the fringe field function.

The field fall-off shape is shown in Fig. 3, representing the vertical magnetic field across a vFFA magnet as a function of the longitudinal coordinate in the midplane (horizontal coordinate = 0) and with zero vertical coordinate. This magnet is of length $L = 0.4\,\text{m}$, has a nominal field of $B_0 = 2.5\,\text{kG}$, and is located at $XM = 65\,\text{cm}$ in a 2.5 m XE+XL+XS extent patch (Fig. 2). The figure shows the superposition of the analytically calculated fringe field function (Eq. (7)) and the field along a straight line crossing a vFFA element when the vertical and horizontal particle coordinates are imposed on remaining identically zero. The field will be equal to $B_0 \times g(x)$ for a zero vertical coordinate and is thus proportional to the fringe field function.

2.2. Full field at arbitrary position

The implemented procedure allows having several vFFA magnets in an element. It is necessary to consider the overlapping contributions of these N neighboring magnets. The magnetic field and derivatives are thus calculated by adding the N-tuple vFFA magnet contributions, as it is done for the "FFAG" and "FFAG-SPI" keywords [15,19]:

$$\mathbf{B}(X,Y,Z) = \sum_{i=1,N} \mathbf{B}_i(X,Y,Z) \tag{8}$$

$$\frac{\partial^{k+l+m}\mathbf{B}(X,Y,Z)}{\partial X^k \partial Y^l \partial Z^m} = \sum_{i=1,N} \frac{\partial^{k+l+m}\mathbf{B}_i(X,Y,Z)}{\partial X^k \partial Y^l \partial Z^m} \tag{9}$$

For each magnet, the field is given everywhere in the 3D volume. The model already considers Maxwell's equations for the magnetic field out of the median plane. As already mentioned, the procedure also allows the linear superposition of sufficiently small residual magnetic fields of neighboring cells using the XE and XS parameters to set the integration limits.

Fig. 4 illustrates how the different sector contributions are accounted for in a vFFA element. The field distribution at different

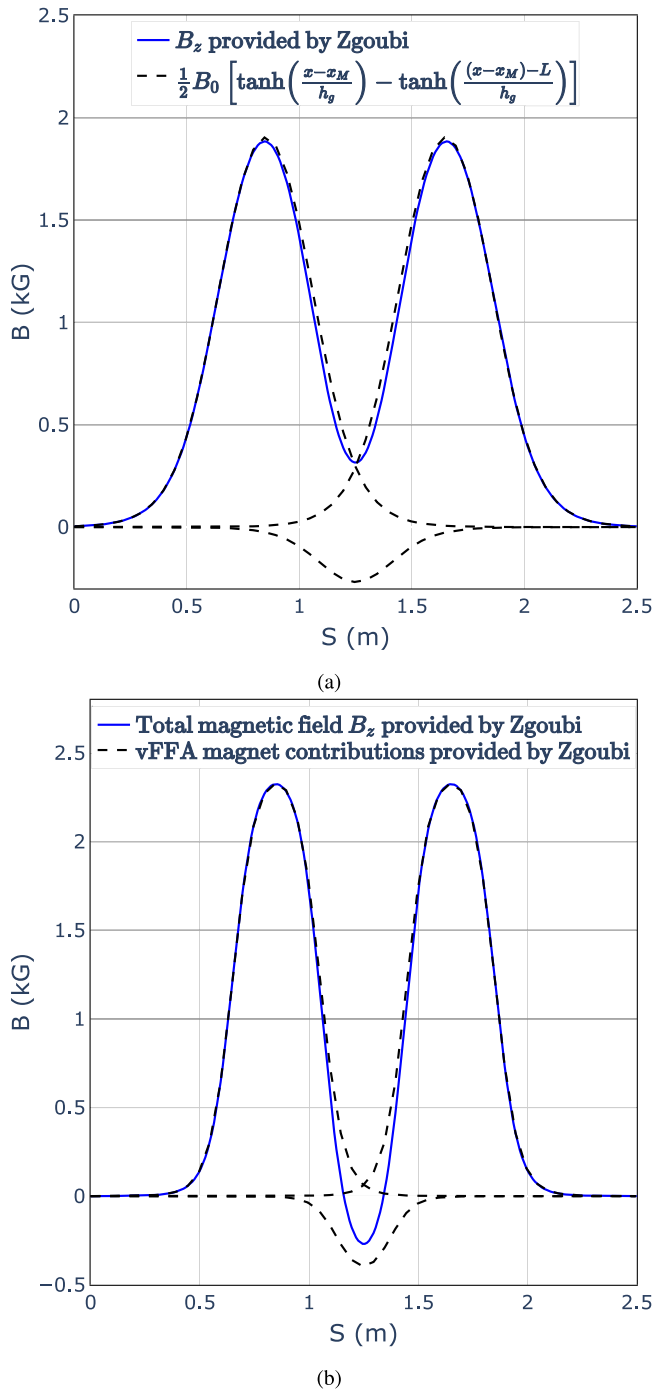

Fig. 4. Vertical magnetic field along a straight line crossing the FDF triplet cell described in Ref. [2]. The central magnet has a negative field dipole, while the two outer magnets are positive field magnets; their normalized field gradient is $1.28\,\mathrm{m}^{-1}$. The horizontal coordinate of the particle is (a) 0 cm (median plane field) and (b) −15 cm. The dashed curves correspond to the field of each magnet individually, while the solid curve corresponds to the superposition of all the sector contributions.

horizontal coordinates is illustrated for the lattice example. The cell is composed of a vFFA triplet whose characteristics are drawn from Ref. [2] and are shown in Table 1. Fig. 4 shows the vertical component of the magnetic field for the three magnets individually and the superposition of these three fields along a straight line through the cell.

The superposition of the field contributions of the vFFA magnets is linear. The final goal of this method is to match it to a realistic field provided by magnet code or measurement. The linear superposition approximation of neighboring magnet fields from analytical models or field maps is a regularly used technique in Zgoubi, which has already shown its effectiveness even for magnets that can be saturated. For example, in Ref. [15], the analytical models of dipoles are linearly superimposed in the Zgoubi "DIPOLES" keyword (which uses the same principle as in the newly implemented vFFA) to study the KEK 150 MeV FFAG. It reproduces a field profile very close to an OPERA calculation of the triplet, as illustrated in Fig. B.1 of Ref. [15]. The validation procedure in Section 3 compares the particle tracking in the vFFA element implemented in Zgoubi (dedicated vFFA keyword) and the tracking in a semi-analytical field map previously generated by the user. The field map is based on the same analytical expressions but only gives the magnetic field at specific points in the 3D space. Tracking in a field map is closer to what will be done in the later stages of machine design and validation. Having similar results with both methods gives confidence in their use: first using the vFFA procedure in the design phase (particularly for optimizing the magnet parameters), then using the tracking in a constructed or measured field map for the final lattice study.

2.3. Field derivatives

Two methods exist in Zgoubi to compute the field derivatives at each integration step. The first one consists in giving the analytical expressions of the magnetic field derivatives at any point in the 3D space. The second one is based on numerical interpolation from the knowledge of the magnetic field on a $n \times n$ flying grid centered on the calculation point. This method is CPU time-consuming because it requires calculating the magnetic field on the $n \times n$ nodes at each integration step. In the vFFA procedure, only the fully analytical method has been implemented as it is faster, more accurate, and shows excellent symplecticity. However, the numerical method is very close to the case of field map tracking. The polynomial interpolation involved for the tracking in field maps is the following [16]:

$$\begin{aligned} B_l(X,Y,Z) = {} & A_{000} + A_{100}X + A_{010}Y + A_{001}Z \\ & + A_{200}X^2 + A_{020}Y^2 + A_{002}Z^2 \\ & + A_{110}XY + A_{101}XZ + A_{011}YZ, \end{aligned} \tag{10}$$

implying that the derivatives can directly be retrieved from this interpolation. By comparing the derivatives obtained in the field map method and the derivatives obtained in the completely analytical method, we thus compare both methods and fully validate the vFFA procedure implementation.

The method used for the vFFA procedure being the analytical one, the magnetic field and its derivatives up to the 2nd-order are set in the Fortran source code for each magnet before adding all the magnet contributions. The source code contains the explicit analytical expressions of specific derivatives ($\partial B_x/\partial x$, $\partial B_x/\partial y$, $\partial B_y/\partial y$, $\partial B_z/\partial x$, $\partial B_z/\partial y$, $\partial^2 B_x/\partial^2 x$, $\partial^2 B_y/\partial^2 y$, $\partial^2 B_x/\partial x \partial y$, $\partial^2 B_x/\partial^2 y$, $\partial^2 B_x/\partial z \partial x$, $\partial^2 B_x/\partial z \partial y$, $\partial^2 B_y/\partial z \partial y$), whereas all the other derivatives stem from Maxwell's equations. As mentioned before, the analytical expressions set in the Fortran source code are obtained with the Python library Sympy and can be readily adapted for further magnetic field improvement.

Although the analytical method allows overcoming the issue of the mesh size dependence, facilitating optimization with the build-in fit procedure, and performing long-term tracking and DA calculations due to its speed, the field map method allows readily changing the field dependence on parameters and evaluating the influence of this change on the lattice design. Using a field map requires reading the magnetic field and interpolating at each integration step and can be CPU time-consuming for the field map generation but allows more flexibility as to possible changes in the magnetic field to account for magnetic errors or shims. Fig. 5 shows the superposition of the derivatives obtained with Zgoubi's dedicated vFFA procedure and obtained with the field map method along the reference trajectory for the vFFA triplet lattice

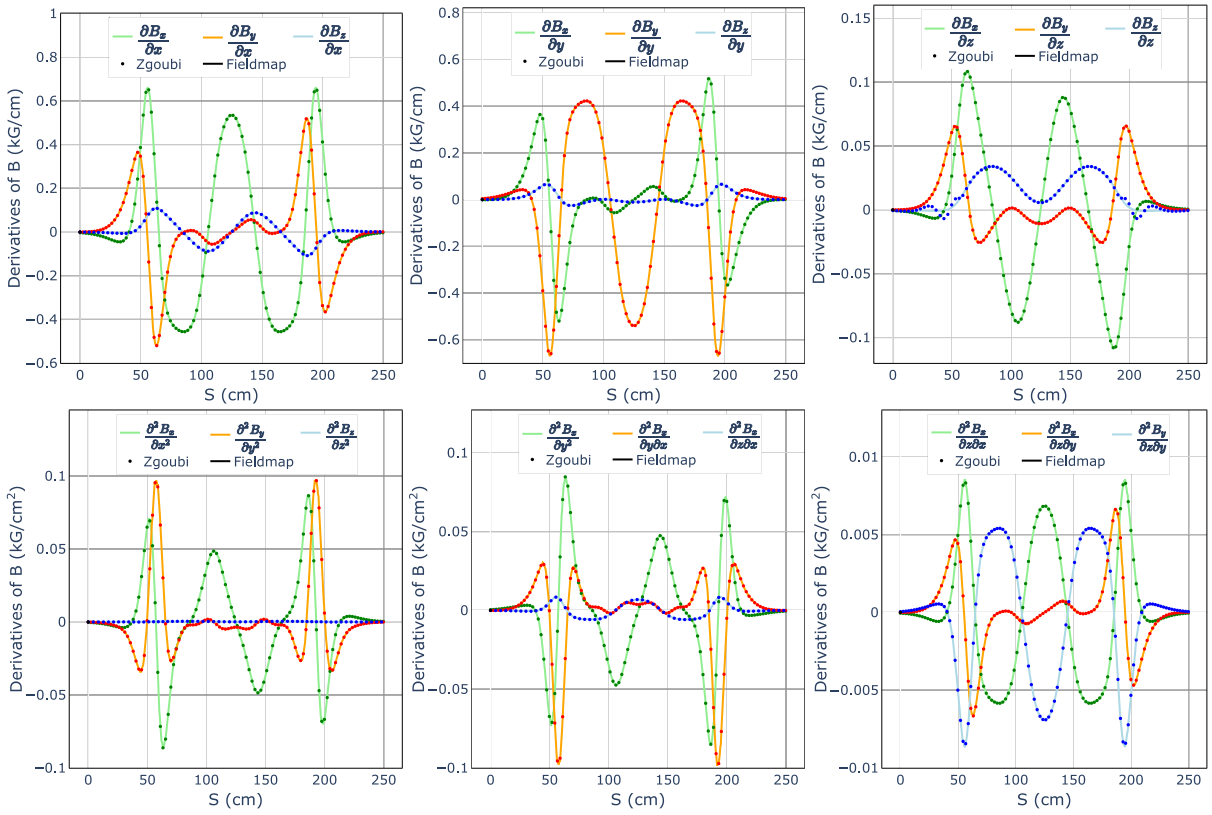

Fig. 5. First and second derivatives along the reference trajectory in the vFFA triplet structure lattice for a particle at 3 MeV. The derivatives returned by Zgoubi for the implemented vFFA procedure and the field map method show good agreement, except for the derivative of the component B_z to z (top-right figure). The difference between both methods reflects a difference between the actual field derivative and the derivative calculated assuming the field Maxwellian character. For the analytical method, the derivative $\partial B_z/\partial z$ is obtained from $\partial B_x/\partial x$ and $\partial B_y/\partial y$ using Maxwell's equations. By contrast, for the field map method, $\partial B_z/\partial z$ is calculated explicitly based on the second-order field map interpolation. There is a slight field component and derivative alteration due to the finite truncation of the magnetic field out-of-plane expansion. This alteration implies that the field is no longer quite Maxwellian at high distances from the median plane.

example. Both methods show good agreement, with the exception of the derivative of the component B_z to z. The difference between both methods reflects a difference between the actual field derivative and the derivative calculated assuming the field Maxwellian character, as explained in more detail in Section 3.1. This difference originates from the slight field component and derivative alteration due to the finite truncation of the magnetic field out-of-plane expansion.

3. Beam dynamics in a vFFA ring.

In this section, the vFFA development in Zgoubi is tested on a lattice whose design is detailed in Ref. [2]. The objective is to demonstrate the validity of the procedure and its efficiency in studying the beam dynamics of vFFA machines. The vFFA procedure has not yet been used to design a lattice. Still, the magnetic field model implemented analytically in Zgoubi makes it possible to optimize the parameters of a lattice easily and to carry out the optics and design study efficiently. The validation procedure was performed by comparing the results obtained with the dedicated vFFA keyword (complete analytical method) and those obtained with particle tracking in field maps (semi-analytical method using the Zgoubi "TOSCA" keyword [16]). The latter approach implies creating a field map. There is an additional step compared to the complete analytical method. However, it is a closer approach to what could be used after the design study: a field map containing a more realistic fringe field or measured field map. Excellent agreement was found between both methods, showing that the additional step does not influence the results. The field map method makes it possible to use realistic fields in the lattice analysis.

The lattice considered in this section is the 10-cell vFFA prototype lattice from Ref. [2]. It is a triplet focusing lattice (FDF) whose magnets

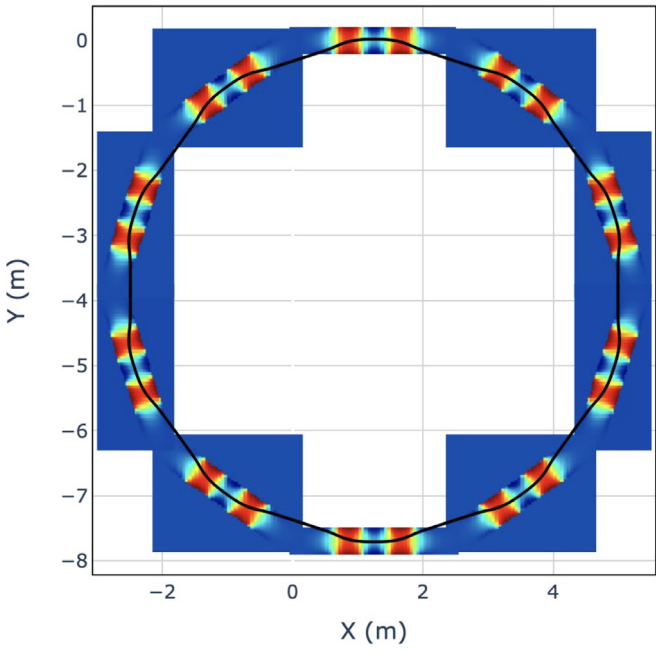

Fig. 6. Magnetic field map of the entire vFFA ring. The closed orbit is shown in black. The orbit excursion with energy is vertical; the closed orbits for different energies are stacked vertically on top of each other. The lattice with 10 FDF cells is visible. The bending angle is 36 degrees per cell.

Table 1
Parameters of the vFFA example ring considered for the validation of the vFFA procedure implemented in the ray-tracing code Zgoubi. The design parameters come from Ref. [2].

Parameters	
Number of cells	10
Cell length	2.5 m
Bd magnet length	0.24 m
Bf magnet length	0.40 m
Space between Bd and Bf	0.08 m
Fringe field extent	0.20 m
Normalized field gradient	1.28 m^{-1}

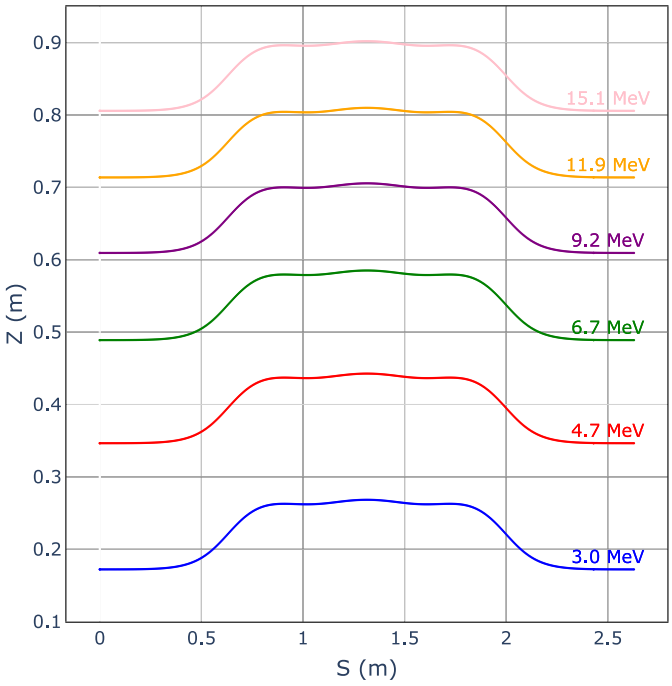

Fig. 7. Periodic closed orbit across a cell, for different energies ranging from 3 to 15 MeV for the vFFA prototype ring example. The vertical orbit excursion is clearly visible.

are aligned on a straight line. The strong focusing is ensured by the cell structure (alternating field) and edge focusing due to the fringe fields. The design parameters are shown in Table 1, and the ring is shown in Fig. 6. All the following results are obtained using Zgoubi combined with its python interface Zgoubidoo [22].

3.1. First order behavior

Fig. 7 shows the vertical closed orbits corresponding to different energies. The vertical orbit excursion is visible; the orbits are stacked vertically, leading to a finite vertical dispersion and zero horizontal dispersion. As expected in a scaling lattice, the single-cell eigentunes are constant over the whole energy range ($\nu_1 = 0.2162$, $\nu_2 = 0.1335$). The magnetic field components along the 3 MeV particle closed orbit are displayed in Fig. 8. The magnetic field interpolated at each integration step in the field map or the one computed analytically are identical, as well as the particle trajectory as shown in Fig. 9.

The peculiar shape of the magnetic field, including the longitudinal component at the magnet edges and the skew quadrupole components in the magnet body, induces strongly coupled optics. In the linear approximation, the lattice functions must be computed with an adequate coupling parametrization, as explained in Ref. [23]. Fig. 10 shows the β-functions from the Lebedev and Bogacz parametrization [24] computed on one cell of the vFFA prototype ring example.

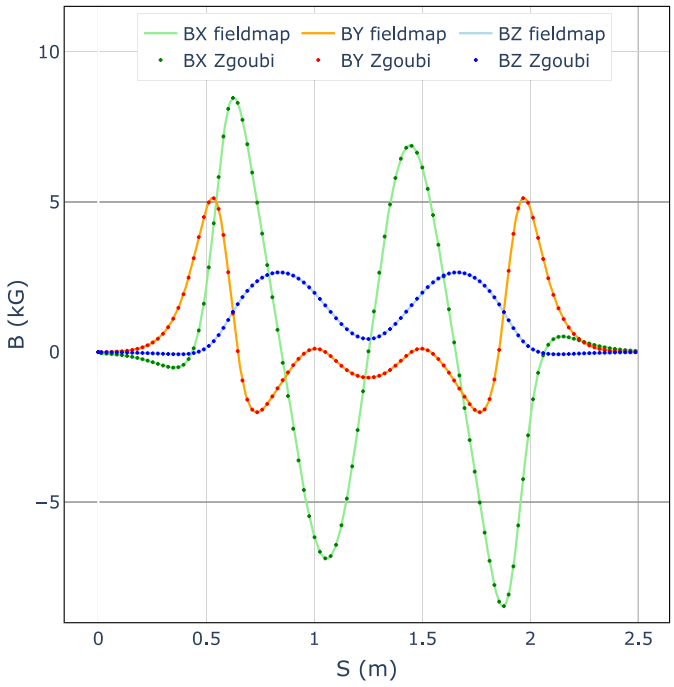

Fig. 8. Magnetic field components along the 3 MeV particle closed orbit for the analytical and field map methods. Both methods give identical results. The polynomial interpolation used in the field map method to compute the magnetic field at each integration step properly restitutes the magnetic field seen by the particle.

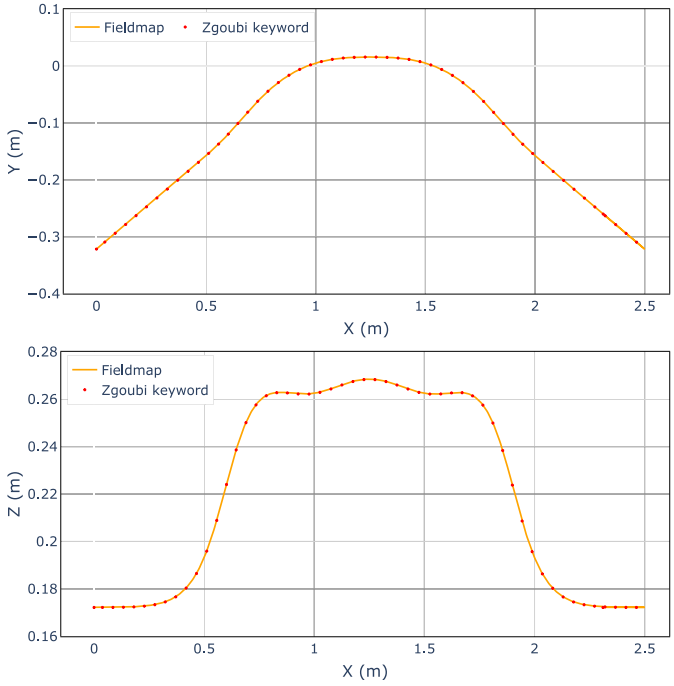

Fig. 9. Comparison between the horizontal and vertical trajectories of a 3 MeV particle for the analytical method ("Zgoubi keyword") and the field map method. Both methods provide the same results.

Accounting for the transverse motion coupling, the tunes computed in the linear beam study are the eigentunes — the tunes of the motion in the linearly decoupled axes. To ensure the results computed with our procedure are correct, we have compared the tunes obtained with Zgoubi with those obtained with other codes (OPAL, FixField, and SCODE) [2]. The tunes are computed from a turn-by-turn frequency

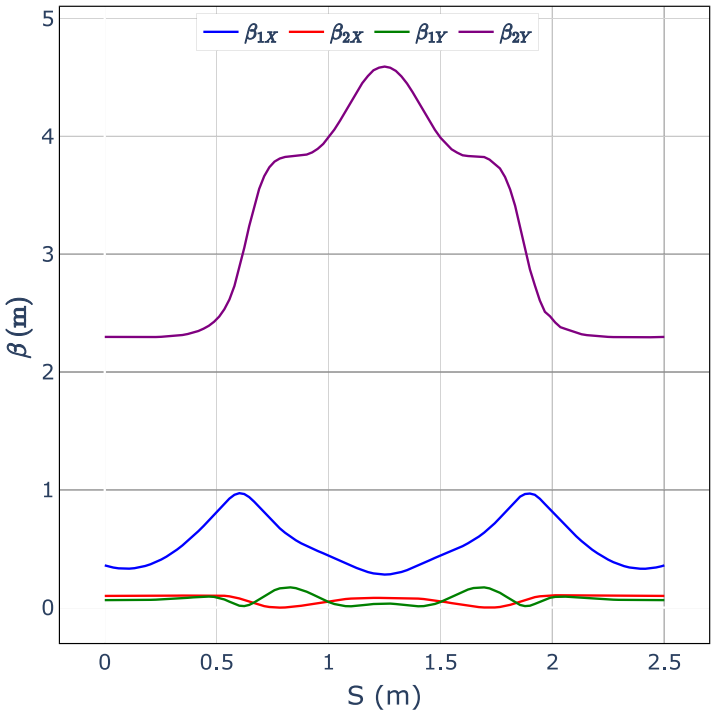

Fig. 10. Coupled β-functions from the Lebedev and Bogacz parametrization [23,24], computed on a cell of the vFFA prototype ring example.

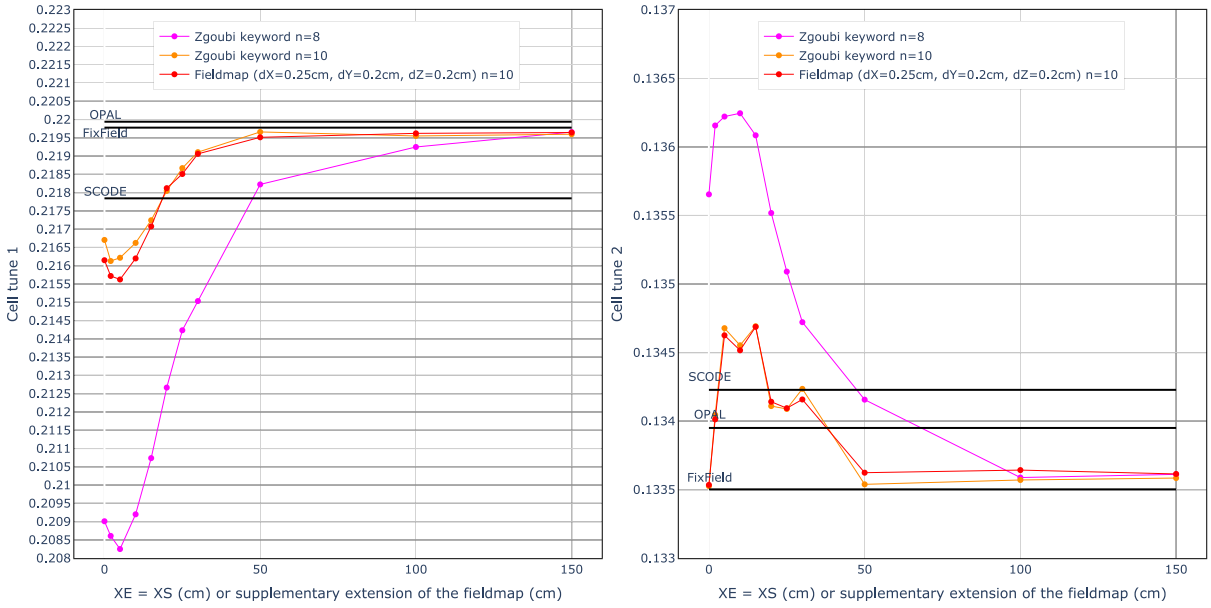

Fig. 11. Computation of the eigentunes dependence on the length of the extended integration zone for mode 1 (left) and mode 2 (right). The tunes are computed from a turn-by-turn frequency analysis over 2000 turns, with an initial horizontal offset of 1 mm. The parameters XE and XS have identical values, and the integration step size is 0.4 cm. As the XE parameter increases, the integration zone increases. It allows increasingly accounting for the residual field of the neighboring cells in the case where the deviation induced by this residual field is sufficiently low such that the linear superposition of the fields is valid. In the case of field maps, increasing the integration zone is equivalent to taking larger extension field maps. With more residual fields considered, the eigentunes converge towards those obtained with FixField. The tune values of SCODE, OPAL, and FixField (provided in Ref. [2]) are represented by straight lines (black) to indicate the convergence of the Zgoubi results to values similar to those obtained in other codes. The values obtained using the analytical method with Taylor series truncation at the 8th order are shown in magenta, the ones using the analytical method with Taylor series truncation at the 10th order are shown in orange, while the ones using the field map method with an out-of-plane expansion at the 10th order for the magnetic field components on the pre-defined mesh are shown in red.

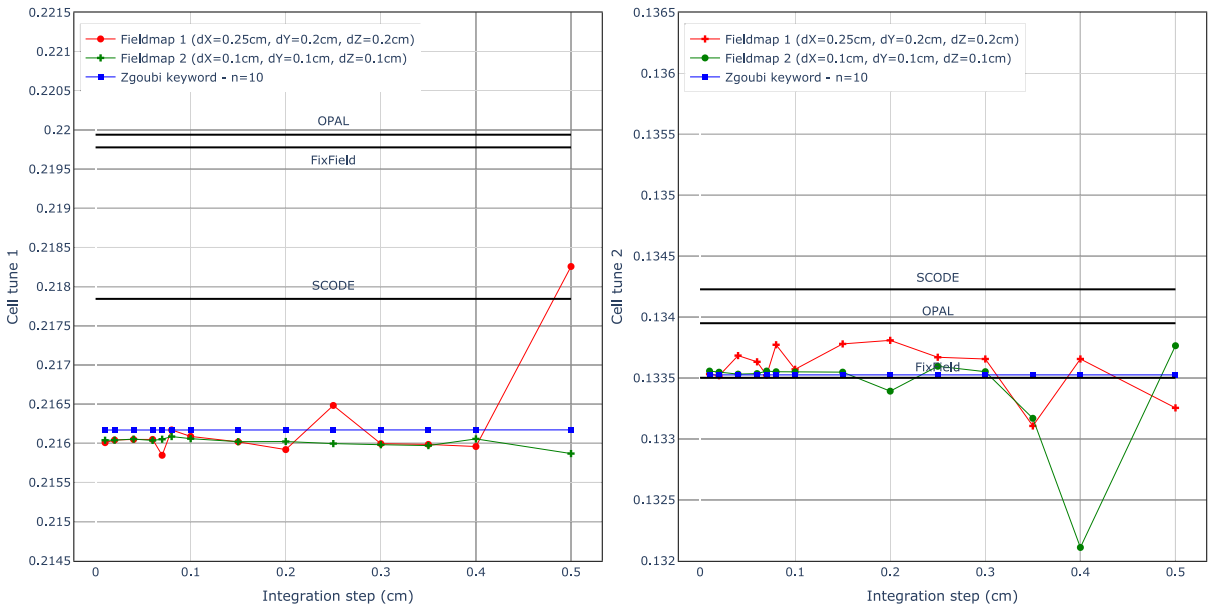

Fig. 12. Dependence of the eigentunes on the integration step. The tunes are retrieved from the one-cell periodic transfer matrix obtained from the tracking results in the Frenet–Serret reference frame. The implemented vFFA procedure based on analytical expressions for the field computation at each integration step is much less dependent on the integration step than the field map method. This latter method shows sensitivity to the integration step and a possible interplay between the integration step and the field map mesh's size. The influence of neighboring cells is not taken into account in this figure (XE = XS = 0).

analysis (FFT of the signal with interpolation method [25]) on 2000 turns, with an initial horizontal offset of 1 mm. The overlapping fringe fields of neighboring cells impact the tunes. To take into account the residual fields of neighboring cells using the implementation of the vFFA keyword, one can set the integration zone to an extent larger than the nominal cell length using the XE and XS parameters (Fig. 2). Zgoubi integrates from -XE to XL+XS, which makes it a valid linear superposition of the neighboring cell residual fields if the orbit deviation due to the residual field is not too large. However, Zgoubi does not provide this capability when using field map elements. To recover this capability, the approach chosen is to explicitly add negative drifts at both cell ends to account for the larger field map extension while keeping constant the total cell length for the placement of the following elements. Similarly to the method used for the analytical vFFA keyword, this method is valid only for sufficiently small residual fields so that the particle trajectory deviation is limited. By varying such integration limits, one can see the increasing influence of neighboring cells on the cell eigentunes. The tune dependence on increasing integration limits or equivalently increasing field map extension is shown in Fig. 11. As more and more residual field is taken into account, the magnetic field changes, and this field change causes an orbit change. This orbit change leads to a focusing change which results in tune variation. The significant sensitivity of the tunes to the fringe field has already been observed previously on other conventional FFA lattices [15]; it is therefore not surprising that the residual field of neighboring cells influences the tunes. Fig. 11 shows that the perturbative effect of the fringe field is significant in the studied machine. The dependence of the SCODE+, OPAL, and FixField tunes on the integration limits is not given in Ref. [2]. We represented their values by straight lines to indicate the convergence of the Zgoubi results (obtained with the dedicated vFFA procedure and with field maps) to values similar to those obtained in other codes. We computed the tunes for truncation of the Taylor series (Eqs. (4)–(6)) at the 8th and 10th order. Although the final convergence values are similar, the tune dependences on the integration limits are quite different. This shows the importance of explicitly implementing an out-of-plane expansion at a sufficiently high order. Finally, there is a good agreement between the analytical and field map tracking methods, and both results are in good agreement with Ref. [2], validating the implemented procedure. The only notable

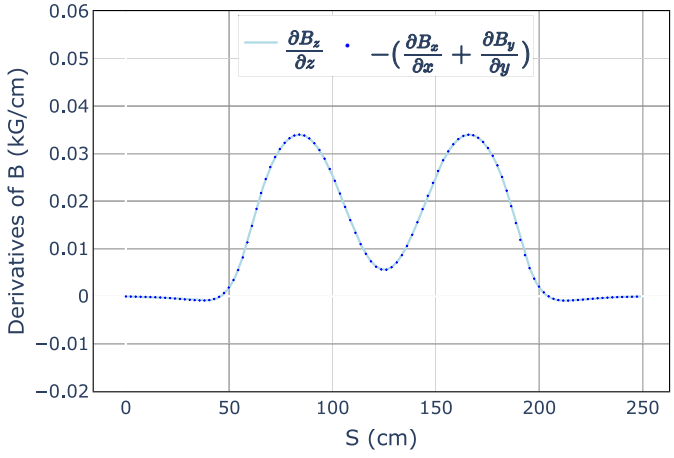

Fig. 13. Comparison of the derivative $\partial B_z/\partial z$ with $-(\partial B_x/\partial x + \partial B_y/\partial y)$ in the case of a field map with an out-of-plane expansion at the 20th order for the magnetic field components on the pre-defined mesh. Comparing the two curves allows comparing the actual derivative with the one computed from Maxwell's equations. The perfect match of the curves indicates that the field is closely Maxwellian for a high-order truncation of the magnetic field out-of-plane expansion.

difference in the results is the greater sensitivity of the field map method to the mesh size and the integration step, as illustrated in Fig. 12. It shows the dependence of eigentunes on the integration step without considering the residual field of neighboring cells (XE = 0, XS = 0). For this figure, the tunes are retrieved from the one-cell periodic transfer matrix obtained from the tracking results in the Frenet–Serret reference frame. The tunes remain almost constant for the implemented vFFA Zgoubi keyword, while they vary for the field map method.

Another remark about the Taylor series truncation for the out-of-plane expansion concerns the Maxwellian character of the field. To notice the alteration of the Maxwellian character with the truncation order, one can observe the derivative of the vertical component of the field with respect to the vertical coordinate $\partial B_z/\partial z$. For the analytical method, this derivative is deduced from Maxwell's equations: $\partial B_z/\partial z = -(\partial B_x/\partial x + \partial B_y/\partial y)$, with $\partial B_x/\partial x$ and $\partial B_y/\partial y$ given explicitly in the

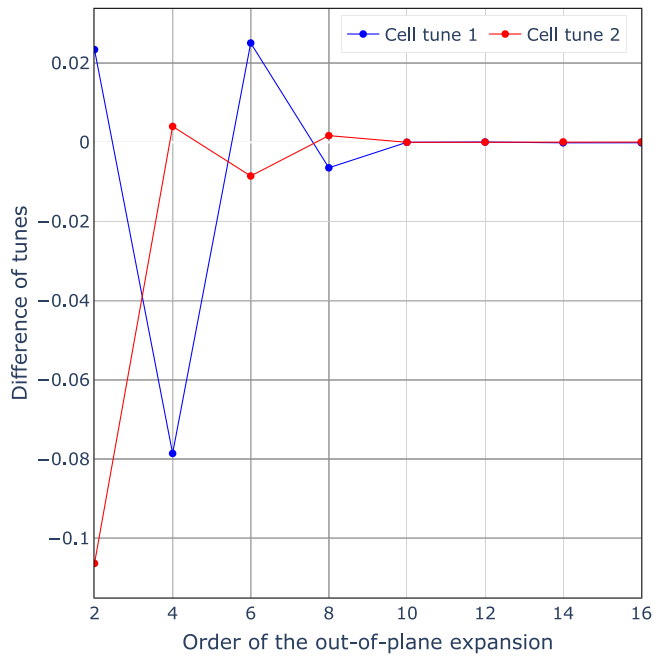

(a)

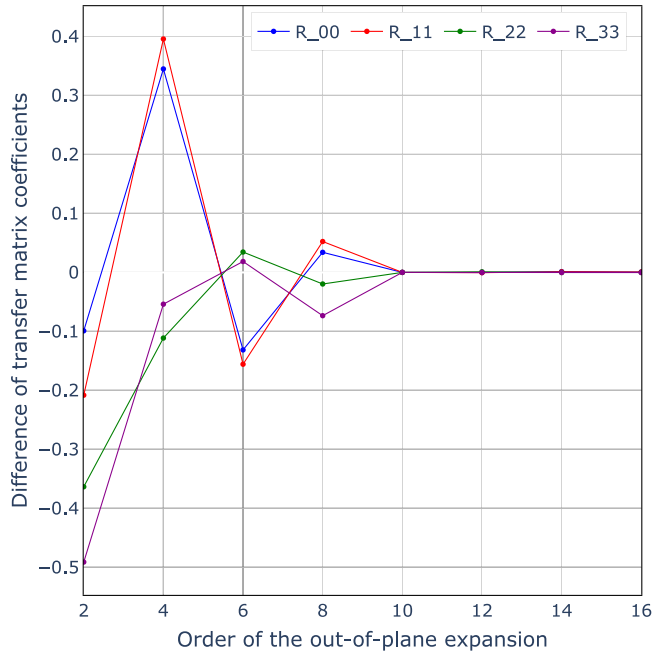

(b)

Fig. 14. Deviation of the eigentunes (a) and transfer matrix coefficients (b) from those computed at the 10th order of truncation for the out-of-plane expansion.

Fortran code. In contrast, for the field map method, it is calculated explicitly based on the interpolation given by Eq. (10). In Fig. 5, we can see a notable difference between these two approaches for $\partial B_z/\partial z$ when the series of Eqs. (4)–(6) is truncated at the 10th order. It indicates a slight alteration of the field Maxwellian character when the particle is far from the vertical midplane (large horizontal coordinates). Implementing the analytical procedure for higher truncation orders in the Fortran source code proves difficult. Still, we can easily generate field maps for higher truncation orders by following the method developed in Ref. [26] to speed up the field map generation procedure. Fig. 13 compares the derivative $\partial B_z/\partial z$ with $-(\partial B_x/\partial x + \partial B_y/\partial y)$ in the case of a field map whose out-of-plane expansion truncation is in the 20th

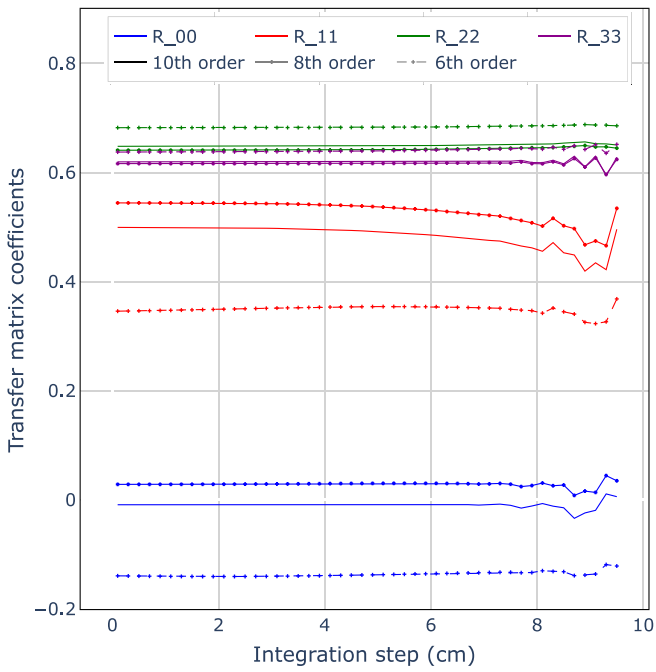

Fig. 15. Dependence of the transfer matrix coefficients on the integration step for different truncation orders. Lower truncation order gives lower coefficient precision but does not affect the convergence with the integration step.

order. There is no longer any difference between both curves, indicating that the field is closely Maxwellian for a high-order truncation of the magnetic field out-of-plane expansion. This observation shows the limits of the vFFA analytical procedure implemented in Zgoubi. The magnetic field can be slightly distorted if the particle is far from the median plane. However, we could see that this slight alteration of the field does not impact the observables, such as the particle trajectory or the linear optics. The analytical model is thus still sufficiently correct to determine the optimal values of the cell parameters using the Zgoubi fitting method.

A convergence study of the eigentunes and transfer matrix coefficients with the truncation order was performed to ensure that the out-of-plane expansion can be safely truncated at the 10th order without inducing too large errors. Field maps were generated at different truncation orders up to n = 16. Fig. 14(a) shows the deviation of the eigentunes for different truncation orders from the eigentunes computed at n = 10. The error is significant for low truncation orders, but the eigentunes converge from the 10th order onwards. The eigentune variations from the 10th to the 16th order are $\Delta\nu_1 = -1.17\ 10^{-4}$, $\Delta\nu_2 = 8.26\ 10^{-5}$, which is beyond the required accuracy. Fig. 14(b) shows the convergence of transfer matrix coefficients with the truncation order by emphasizing the deviation of these coefficients from those computed for n = 10. Again, convergence is reached at the 10th order, which shows that this truncation order is adequate for implementing the analytical procedure in Zgoubi.

Finally, Fig. 15 shows the transfer matrix coefficient dependence on the integration step for different orders of the out-of-plane expansion truncation in the analytical method. Although the coefficients converge for the same integration step with the 6th, 8th, and 10th order truncation for the analytical method, the precision of the coefficients seems affected by the truncation at a lower order, as we have already observed before. There is also a loss of precision if the integration step is too large. It is necessary to take an integration step small enough to ensure the step-by-step numerical integration precision but large enough to reduce the computation time.

The linear dynamics results and validation of the newly implemented vFFA Zgoubi keyword against previous results prove the efficiency of the vFFA procedure combined with the Zgoubi particle

tracking numerical techniques to study completely vertical orbit excursion rings. It paves the way for further in-depth studies of these rings, particularly the study of large amplitude transverse motion and 6D-tracking by considering the ring acceleration cycle.

4. Conclusion

A vFFA procedure that allows particle tracking in the vFFA complex non-linear magnetic field has been implemented in the ray-tracing code Zgoubi. The method includes the neighboring magnet field superposition and the superposition of adjacent cell residual fields. The procedure considers hyperbolic tangent fringe fields, but it is planned to adjust the model when in-depth studies concerning realistic magnet fringe fields are completed. A detailed comparison between Zgoubi's analytical model and the 3D magnetic field from magnet code will have to be carried out. The canvas already implemented in Zgoubi, together with the external Python Sympy code allowing to obtain the field analytical expressions, makes it straightforward to adapt the magnetic field to other fringe field shapes and field models. The method implemented in Zgoubi is completely analytical, allowing fast-tracking and optimizing parameters using Zgoubi fitting method. The vFFA method has been successfully used to thoroughly investigate the linear beam dynamics of a vFFA prototype ring, including the closed orbit search for different energies and the computation of eigentunes. The results show excellent agreement with prior results from the design study using other simulation codes. The analytical method was also compared and validated with particle tracking in 3D semi-analytical field maps. The additional step between the magnetic field computation and the particle tracking has not influenced the linear optics results. We can therefore use the analytical method for design studies before using particle tracking in field maps for the later stages of the vFFA machine study. The analytical approach limits are reached for large distances from the median plane. Because of the out-of-plane expansion truncation, the field is slightly altered, but the main results seem not to be too much affected. The eigentunes and transfer matrix coefficients converge for truncation at the 10th order, which is thus adequate for the Zgoubi vFFA analytical procedure. The analytical and field map methods show excellent symplecticity and can be used extensively for further studies of vFFA machines.

CRediT authorship contribution statement

Marion Vanwelde: Conceptualization, Methodology, Software, Validation, Investigation, Writing – original draft, Writing – review & editing. **Cédric Hernalsteens:** Conceptualization, Methodology, Supervision, Writing – original draft, Writing – review & editing. **François Méot:** Methodology, Software, Writing – review & editing. **Nicolas Pauly:** Supervision, Writing – review & editing. **Robin Tesse:** Software, Writing – review & editing.

Declaration of competing interest

The authors declare that they have no known competing financial interests or personal relationships that could have appeared to influence the work reported in this paper.

Data availability

Data will be made available on request.

Acknowledgments

The authors would like to thank D. Kelliher, J.-B. Lagrange and S. Machida for their support and the many fruitful discussions. Marion Vanwelde is a Research Fellow of the Fonds de la Recherche Scientifique – FNRS. This work is supported by Brookhaven Science Associates, LLC under Contract No. DE-AC02-98CH10886 with the U.S. Department of Energy.

References

[1] S. Brooks, Vertical orbit excursion fixed field alternating gradient accelerators, Phys. Rev. ST Accel. Beams 16 (8) (2013) 084001.
[2] S. Machida, D.J. Kelliher, J.-B. Lagrange, C.T. Rogers, Optics design of vertical excursion fixed-field alternating gradient accelerators, Phys. Rev. Accel. Beams 24 (2) (2021) 021601.
[3] J. Thomason, et al., ISIS II "Working Group Report", https://www.isis.stfc.ac.uk/Pages/isis-iiworking-group-report16266.pdf.
[4] C.M. Warsop, et al., Studies for major ISIS upgrades via conventional RCS and accumulator ring designs, in: Proc. IPAC'18, JACoW Publishing, Geneva, Switzerland, pp. 1148–1150.
[5] J.-B. Lagrange, et al., Progress on design studies for the ISIS II upgrade, in: Proc. IPAC'19, JACoW Publishing, Geneva, Switzerland, pp. 2075–2078.
[6] S. Machida, FFA options for ISIS upgrade and the feasibility study, in: Proc. 3rd J-PARC Symposium, J-PARC2019, Tsukuba, Japan, 2021, 011005, http://dx.doi.org/10.7566/JPSCP.33.011005.
[7] F. Méot, The ray-tracing code Zgoubi, Nucl. Instrum. Methods Phys. Res. A 427 (1–2) (1999) 353–356.
[8] F. Méot, The ray-tracing code Zgoubi – Status, Nucl. Instrum. Methods Phys. Res. A 767 (2014) 112–125.
[9] F. Méot, J.S. Berg, Zgoubi, 2020, http://sourceforge.net/projects/zgoubi/.
[10] S. Machida, Modelling of a nonscaling FFAG and findings with the new code, ICFA BD Newslett. 43 (54) (2007).
[11] J.-B. Lagrange, R.B. Appleby, J.M. Garland, J. Pasternak, S. Tygier, Racetrack FFAG muon decay ring for nuSTORM with triplet focusing, J. Instrum. 13 (09) (2018) P09013.
[12] F. Meot, RACCAM: An example of spiral sector scaling FFA technology, Technical Report BNL–211536-2019-NEWS, 1507116, 2019.
[13] S. Machida, et al., Acceleration in the linear non-scaling fixed-field alternating-gradient accelerator EMMA, Nat. Phys. 8 (3) (2012) 243–247.
[14] K.J. Peach, et al., Conceptual design of a nonscaling fixed field alternating gradient accelerator for protons and carbon ions for charged particle therapy, Phys. Rev. ST Accel. Beams 16 (3) (2013) 030101.
[15] F. Lemuet, F. Méot, Developments in the ray-tracing code Zgoubi for 6-D multiturn tracking in FFAG rings, Nucl. Instrum. Methods Phys. Res. A 547 (2–3) (2005) 638–651.
[16] F. Méot, Zgoubi Users' Guide, Technical Report BNL-98726-2012-IR, https://sourceforge.net/p/zgoubi/code/HEAD/tree/trunk/guide/Zgoubi.pdf.
[17] A. Adelmann, et al., OPAL a versatile tool for charged particle accelerator simulations, 2019, arXiv:1905.06654.
[18] S. Agostinelli, et al., Geant4—a simulation toolkit, Nucl. Instrum. Methods Phys. Res. A 506 (3) (2003) 250–303.
[19] J. Fourrier, F. Martinache, F. Méot, J. Pasternak, Spiral FFAG lattice design tools. Application to 6-D tracking in a proton-therapy class lattice, Nucl. Instrum. Methods Phys. Res. A 589 (2) (2008) 133–142.
[20] J.-B. Lagrange, VFFA magnet prototype, International Workshop on Fixed Field alternating gradient Accelerators, FFA'21, Kyoto, Japan, 2021.
[21] A. Meurer, et al., Sympy: symbolic computing in Python, PeerJ Comput. Sci. 3 (2017) e103.
[22] C. Hernalsteens, R. Tesse, M. Vanwelde, Zgoubidoo, 2022, https://ulb-metronu.github.io/zgoubidoo/.
[23] M. Vanwelde, C. Hernalsteens, S.A. Bogacz, S. Machida, N. Pauly, Review of coupled betatron motion parametrizations and applications to strongly coupled lattices, 2022, arXiv:2210.11866.
[24] V.A. Lebedev, S.A. Bogacz, Betatron motion with coupling of horizontal and vertical degrees of freedom, J. Instrum. 5 (10) (2010) P100100.
[25] R. Bartolini, A. Bazzani, M. Giovannozzi, W. Scandale, E. Todesco, Algorithms for a Precise determination of the betatron tune, in: Proc. EPAC'96. JACoW Publishing, Geneva, Switzerland.
[26] S. Brooks, Fringe Fields for VFFAG Magnets with Edge Angles (unpublished), http://stephenbrooks.org/ral/report/2011-6/skewVFFAGfringes.pdf.